

---

# A Non-Normal-Mode Marginal State of Convection in a Porous Box with Insulating End-Walls

Peder A. Tyvand · Jonas Kristiansen  
Nøland

Received: date / Accepted: date

**Abstract** The 4th order Darcy-Bénard eigenvalue problem for the onset of thermal convection in a 3D rectangular porous box is investigated. We start from a recent 2D model [1] for a rectangle with hand-picked boundary conditions defying separation of variables so that the eigenfunctions are of non-normal mode type. In this paper, the previous 2D model [1] is extended to 3D by a Fourier component with wavenumber  $k$  in the horizontal  $y$  direction, due to insulating and impermeable sidewalls. As a result, the eigenvalue problem is 2D in the vertical  $xz$ -plane, with  $k$  as a parameter. The transition from a preferred 2D mode to 3D mode of convection onset is studied with a 2D non-normal mode eigenfunction. We study the 2D eigenfunctions for a unit width in the lateral  $y$  direction to compare the four lowest modes  $k_m = m\pi$  ( $m = 0, 1, 2, 3$ ), to see whether the 2D mode ( $m = 0$ ) or a 3D mode ( $m \geq 1$ ) is preferred. Further, a continuous spectrum is allowed for the lateral wavenumber  $k$ , searching for the global minimum Rayleigh number at  $k = k_c$  and the transition between 2D and 3D flow at  $k = k^*$ . Finally, these wavenumbers  $k_c$  and  $k^*$  are studied as functions of the aspect ratio.

**Keywords** Convection · Non-normal mode · Onset · Porous box · Rayleigh-Bénard problem

---

P. A. Tyvand  
Faculty of Mathematical Sciences and Technology  
Norwegian University of Life Sciences  
1432 Ås, Norway  
Tel.: +47-67231564  
E-mail: Peder.Tyvand@nmbu.no

J. K. Nøland (Corresponding Author)  
Faculty of Information Technology and Electrical Engineering  
Norwegian University of Science and Technology  
E-mail: Jonas.K.Noland@ntnu.no

## 1 Introduction

Convection in porous media has its own mathematical advantages. In fact, the differential equations yield a lower spatial order than the convection in fluids. Moreover, the fourth-order eigenvalue problem for the onset of Darcy-Bénard convection has analogies with free vibration of elastic plates, and may possibly be developed in parallel with the more established elasticity theory.

The most important challenge for these fourth-order eigenvalue problems is the local behavior of eigenfunctions near non-analytical corners where a Taylor expansion does not exist. Such behavior is to be expected when general physical boundary conditions are allowed because the fourth-order differential equation does not separate in orthogonal coordinate systems. This non-separability, in combination with non-degenerate boundary conditions, can give rise to singularities at the corners. Moffatt [2] wrote a pioneering paper about the singularities that arise in 2D Stokes flow in corners with the no-slip condition. These so-called Moffatt-vortices are corner singularities that also apply to the equilibrium of clamped elastic plates. It is likely that similar singularities arise in the non-analytical corner of our model. Since the Darcy-Bénard problem is more complicated than mechanical biharmonic problems, the investigation of possible thermo-mechanical corner singularities is left for future investigations.

The present paper is an extension to 3D of the previous TNS paper by Tyvand *et al.* [1]. Free thermal convection in porous media is a topic where the limitations of 2D theory can be handled with ease, but only within the tacit paradigm of normal modes. It is convenient to formulate end-wall boundary conditions compatible with normal modes, to encompass an original 2D model as a zeroth-order lateral mode within a consistent 3D model. This type of extension from 2D to a full 3D theory was first carried out by Storesletten and Tveitereid [3]. They studied the onset of convection in a horizontal porous cylinder with impermeable and conducting cylinder walls, where the end-walls were assumed impermeable and adiabatic.

Horton and Rogers [4] and later Lapwood [5] wrote the pioneering papers on the onset of convection in a porous layer heated from below. The linearized onset problem for a rectangular geometry will be called the HRL problem. Wooding [6] developed the theory for vertical porous cylinders, but his work was limited by the assumption of normal-mode degeneracy in the horizontal cross-section plane.

Beck [7] carried out this 3D normal-mode analysis for a rectangular box. Nield [8] generalized the solution of the HRL problem to non-normal mode dependency in the vertical direction, while his assumption of a infinitely wide layer in the horizontal directions implied a normal-mode dependency horizontally. Nilsen and Storesletten [9] wrote the first paper on an HRL problem where non-normal mode dependency was taken into account in a horizontal direction, but their work was limited to 2D flow. The extension of their work to 3D was given by Barletta and Storesletten [10]. In the present work, we perform a similar extension of a 2D model to 3D, in terms of normal modes in the

perpendicular direction. The 2D model that is extended is the porous rectangle investigated in the TNS paper [1]. This TNS paper established 2D eigenfunctions that are non-separable in space because the boundary conditions are incompatible with normal modes. The present paper is the first theoretical study of an HRL onset problem in a 3D porous enclosure with non-normal mode behavior in a vertical cross-section plane.

## 2 Mathematical formulation

A 3D rectangular porous box is considered. It is bounded by impermeable and insulating walls  $y = 0$  and  $y = \Delta y$ . The lower and upper boundaries of the porous box are  $z = 0$  and  $z = h$ . The  $z$  axis is directed vertically upwards.

The velocity vector  $\mathbf{v}$  has Cartesian components  $(u, v, w)$ . The temperature field is  $T(x, y, z, t)$ , with  $t$  denoting time. There is an undisturbed motionless state with a uniform vertical temperature gradient. The gravitational acceleration  $g$  is written in vector form as  $\mathbf{g}$ . The porous medium is homogeneous and isotropic, with permeability  $K$ . The standard Darcy-Boussinesq equations for free thermal convection can be written

$$\nabla p + \frac{\mu}{K} \mathbf{v} + \rho_0 \beta (T - T_0) \mathbf{g} = 0, \quad (1)$$

$$\nabla \cdot \mathbf{v} = 0, \quad (2)$$

$$(\rho c_p)_m \frac{\partial T}{\partial t} + (\rho c_p)_f \mathbf{v} \cdot \nabla T = \lambda_m \nabla^2 T. \quad (3)$$

In these equations,  $p$  is the dynamic pressure,  $\beta$  is the coefficient of thermal expansion,  $\rho = \rho_0$  is the fluid density at the reference temperature  $T_0$ ,  $\mu$  is the dynamic viscosity of the saturating fluid,  $c_p$  is the specific heat at constant pressure, and  $\lambda_m$  is the thermal conductivity of the saturated porous medium. The subscript  $m$  refers to an average over the solid/fluid mixture, while the subscript  $f$  refers to the saturating fluid alone.

The 3D porous medium is bounded by the six sides

$$x = 0, \quad x = l, \quad y = 0, \quad y = \Delta y, \quad z = 0, \quad z = h. \quad (4)$$

The lower boundary is taken to be perfectly heat-conducting and impermeable

$$T = T_0, \quad w = 0, \quad \text{at } z = 0, \quad (5)$$

while the upper boundary is taken to have a given heat flux while it is impermeable

$$\frac{\partial T}{\partial z} = -\frac{\Delta T}{h}, \quad w = 0, \quad \text{at } z = h. \quad (6)$$

$\Delta T$  is the temperature difference across the layer in its undisturbed state.  $T_0$  is a reference temperature. The left-hand boundary is assumed to be thermally insulating and impermeable

$$\frac{\partial T}{\partial x} = 0, \quad u = 0, \quad \text{at } x = 0, \quad (7)$$

while the right-hand boundary is assumed to be perfectly conducting and impermeable

$$T - T_0 = \frac{\Delta T}{h} z, \quad u = 0, \quad \text{at } x = l. \quad (8)$$

There are two end-walls constraining the 3D flow in the  $y$  direction, where we pose the standard conditions that the walls are thermally insulating and impermeable

$$\frac{\partial T}{\partial y} = 0, \quad v = 0, \quad \text{at } y = 0, \quad (9)$$

$$\frac{\partial T}{\partial y} = 0, \quad v = 0, \quad \text{at } y = \Delta y. \quad (10)$$

These six boundary conditions are handpicked to violate the requirements for normal mode solutions, but only in the  $xz$ -plane. The flow in the  $y$  direction is of normal-mode type and can be separated out to achieve a 2D eigenvalue problem, where the wavenumber  $k$  for the  $y$  direction will be separated out. Our previous TNS paper [1] is devoted to the special case  $k = 0$  where the flow is 2D in the  $xz$ -plane, which will be a possibility when  $\Delta y$  is sufficiently small. Note that it will never be an option to have a 2D flow in the  $yz$ -plane.

*Figure 1* gives definition sketches of the rectangular porous box.

## 2.1 Dimensionless equations

From now on, we work with dimensionless variables. We reformulate the mathematical problem in dimensionless form by means of the transformations

$$\begin{aligned} \frac{1}{h}(x, y, z) &\rightarrow (x, y, z), & \frac{h}{\kappa_m}(u, v, w) &\rightarrow (u, v, w), & h\nabla &\rightarrow \nabla, \\ \frac{1}{\Delta T}(T - T_0) &\rightarrow T, & \frac{K}{\mu\kappa_m}(p - p_0) &\rightarrow p, & \frac{(\rho c_p)_f \kappa_m}{(\rho c_p)_m H^2} t &\rightarrow t, \end{aligned} \quad (11)$$

where  $\kappa_m = \lambda_m / (\rho_0 c_p)_f$  is the thermal diffusivity of the saturated porous medium. We denote the vertical unit vector by  $\mathbf{k}$ , directed upwards.

The dimensionless governing equations can then be written

$$\mathbf{v} + \nabla p - R T \mathbf{k} = 0. \quad (12)$$

$$\nabla \cdot \mathbf{v} = 0 \quad (13)$$

$$\frac{\partial T}{\partial t} + \mathbf{v} \cdot \nabla T = \nabla^2 T, \quad (14)$$

with the boundary conditions at the lower and upper boundaries

$$w = T = 0, \quad z = 0, \quad (15)$$

$$w = \frac{\partial T}{\partial z} + 1 = 0, \quad z = 1. \quad (16)$$

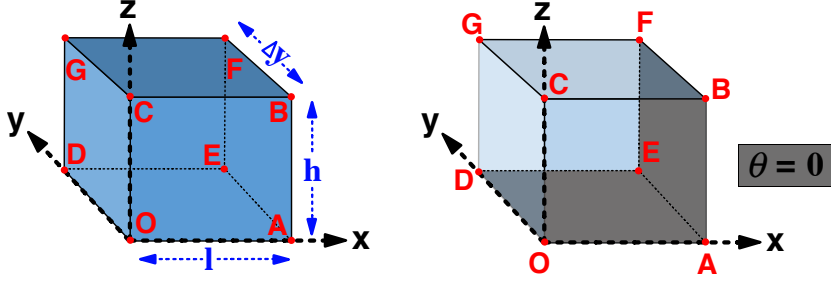


**Fig. 1** Definition sketches of the porous box, with length  $l$ , width  $\Delta y$  and height  $h$ . The lower rectangle is  $OAED$ , and the upper rectangle is  $CBFG$ . The right-hand sketch shows the bottom  $OAED$  and the sidewall  $ABFE$  marked with grey, as thermally conducting boundaries. The thermal condition at the other four walls is the homogeneous Neumann condition  $\partial\theta/\partial n = 0$ . This includes the insulating end-walls  $OABC$  and  $DEFG$ , which allow normal modes in the  $y$  direction. All boundaries are impermeable.

Here the Rayleigh number  $R$  is defined as

$$R = \frac{\rho_0 g \beta K \Delta T h}{\mu \kappa_m}. \quad (17)$$

## 2.2 Basic solution

The stationary basic solution of eqs. (12)-(16) is given subscript "b"

$$\mathbf{v}_b = 0, \quad T_b = -z, \quad p_b = -\frac{1}{2}R z^2. \quad (18)$$

This basic state of hydrostatic fluid has a linear temperature profile.

## 2.3 Linearized perturbation equations

In our stability analysis we disturb the static state (18) with perturbed fields

$$\mathbf{v} = \mathbf{v}_b + \mathbf{v}' = 0 + \mathbf{v}, \quad T = T_b(z) + \Theta, \quad p = p_b(z) + p', \quad (19)$$

with perturbations  $\mathbf{v}', \Theta, p'$  that are functions of  $x, z$  and  $t$ . Linearizing eqs. (12)-(14) with respect to perturbations and eliminating the pressure gives

$$\nabla^2 w = R \nabla_1^2 \Theta, \quad (20)$$

$$\frac{\partial \Theta}{\partial t} - w = \nabla^2 \Theta. \quad (21)$$

We have introduced the two-dimensional operator  $\nabla_1 = (\partial/\partial x, \partial/\partial y)$ . The onset of convection is assumed to occur with a non-oscillatory marginal state. At marginal stability, the heat equation (21) reduces to

$$-w = \nabla^2 \Theta. \quad (22)$$

These coupled second-order equations are combined with homogeneous boundary conditions for  $w$  and  $\theta$ . The general mathematical form for a vector field with zero divergence is

$$\mathbf{v} = \nabla\phi + \nabla \times \boldsymbol{\chi}, \quad (23)$$

applied to our velocity field  $\mathbf{v}$ . We have introduced the velocity potential  $\phi$ , which is zero for the rotational thermo-mechanical flow. The entire flow is therefore given by the vector potential,  $\boldsymbol{\chi}$ , which has the Cartesian coordinates

$$\boldsymbol{\chi} = (\chi_x, \chi_y, \chi_z). \quad (24)$$

The general expression (23) with  $\phi = 0$  is thus equivalent to the mathematical description of magnetic fields. However, from Darcy's law in eq. (12), it follows that  $\nabla \times \mathbf{v}$  does not have a vertical component, which implies that the relationship

$$\frac{\partial^2 \chi_x}{\partial x \partial z} + \frac{\partial^2 \chi_y}{\partial y \partial z} - \nabla_1^2 \chi_z = 0, \quad (25)$$

is valid in the entire fluid domain. The way to achieve this is to introduce the poloidal vector potential  $\Psi$  defined by the relationship

$$\boldsymbol{\chi} = \nabla \times (\Psi \mathbf{k}), \quad (26)$$

so that  $\chi_z$  is identically zero, and the velocity field is given by the scalar function  $\Psi$  as

$$(u, v, w) = \left( \frac{\partial^2 \Psi}{\partial x \partial z}, \frac{\partial^2 \Psi}{\partial y \partial z}, -\nabla_1^2 \Psi \right), \quad (27)$$

satisfying the continuity equation (13).

The perturbation temperature  $\Theta$  is thus given by

$$\Theta = -R^{-1} \nabla^2 \Psi, \quad (28)$$

while the heat equation is rewritten as

$$\nabla^2 \Theta = \nabla_1^2 \Psi. \quad (29)$$

## 2.4 The chosen boundary conditions

We reformulate the above boundary conditions, in terms of the perturbations. The lower boundary is assumed impermeable ( $w = 0$ ) and perfectly heat conducting

$$\nabla_1^2 \Psi = \Theta = 0, \quad z = 0, \quad (30)$$

while the upper boundary is impermeable, with constant given heat flux

$$\nabla_1^2 \Psi = \frac{\partial \Theta}{\partial z} = 0, \quad z = 1. \quad (31)$$

The left-hand sidewall is impermeable ( $u = 0$ ) and thermally insulating

$$\frac{\partial \Psi}{\partial x} = \frac{\partial \Theta}{\partial x} = 0, \quad \text{at } x = 0, \quad (32)$$

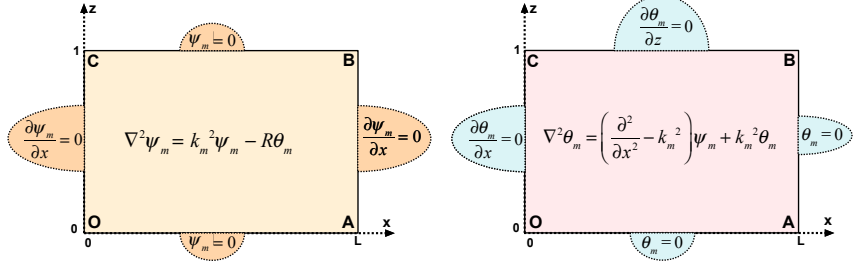


**Fig. 2** Definition of the 2D eigenvalue problem for the vertical cross-section of the porous box.

while the right-hand sidewall is impermeable and perfectly heat conducting

$$\frac{\partial \Psi}{\partial x} = \Theta = 0, \quad \text{at } x = L. \quad (33)$$

We have here introduced the aspect ratio  $L = l/h$ , which is the dimensionless width of the porous rectangle.

The front and rear walls are impermeable ( $v = 0$ ) and thermally insulating

$$\frac{\partial \Psi}{\partial y} = \frac{\partial \Theta}{\partial y} = 0, \quad \text{at } y = 0, \quad (34)$$

$$\frac{\partial \Psi}{\partial y} = \frac{\partial \Theta}{\partial y} = 0, \quad \text{at } y = Y, \quad (35)$$

where we have introduced the dimensionless width  $Y$  of the box in the  $y$  direction, which is  $Y = \Delta y/h$ . In the kinematic boundary conditions for the vertical walls, we have performed an integration in the vertical direction, in order to achieve Neumann conditions for  $\Psi$ . Note the contrast to the Dirichlet condition for representing an impermeable wall with a 2D streamfunction, applied in the TNS paper [1].

### 3 The 3D eigenvalue problem reduced to 2D in $x$ and $z$

The boundary conditions for the  $y$  direction are compatible with normal modes, which means that the  $y$  dependency is degenerate, and we can separate out a Fourier component with the wavenumber  $k = k_m$  in the  $y$  direction for the eigenfunctions, rewriting them as

$$\Psi = \psi_m(x, z) \cos(k_m y), \quad (36)$$

$$\Theta = \theta_m(x, z) \cos(k_m y), \quad (37)$$

where the  $m$ th dimensionless wavenumber in the  $y$  direction is given by

$$k_m = m \frac{\pi}{Y}, \quad m = 0, 1, 2, \dots \quad (38)$$

The lowest mode in the  $y$  direction is represented by  $m = 0$ . This case  $k = 0$  is the 2D case already studied in our previous TNS paper [1], but it does not have to be the preferred mode of convection. If the dimensionless width  $Y$  of the rectangular box is large enough, the preferred mode of convection will be 3D with  $m \geq 1$  and  $k > 0$ .

As illustrated in *Figure 2*, a 2D eigenvalue problem in the  $xz$ -plane can now be formulated for the two coupled eigenfunctions  $\psi_m(x, z)$  and  $\theta_m(x, z)$ . Since the non-negative integer  $m$  is already a parameter that specifies the dependency in the normal direction to the  $xz$ -plane of calculation, there will be a double set of integers for selecting the preferred mode of onset. The 2D modes in the  $xz$ -plane (to be denoted by the positive integer  $n$ ), and the 1D Fourier modes  $k_m$  in the  $y$  direction (denoted by the non-negative integer  $m$ ). Since the solutions of the 2D eigenvalue problem are of non-normal mode type, the number  $n$  is not linked to a spatial direction but to the entire cross-section rectangle in the  $xz$ -plane.

The corner  $B$  is the single non-analytical corner for the 2D thermo-mechanical eigenvalue problem. Its possible singularity is left for future work, as it is even more difficult in 3D than in the previous 2D version [1]. The 2D version has a contradiction in the thermal versus the kinematic boundary condition at the non-analytical corner  $B$ . To the left of the corner  $B$ , the isotherms meet the streamlines at a right angle near the boundary  $BC$ . Below the corner  $B$ , the isotherms are parallel to the boundary near the boundary  $AB$ . This conflict may induce a weak singularity for the temperature perturbation near the corner  $B$ . Since the thermo-mechanical eigenfunctions are strictly coupled, there may also be a singularity for the 2D streamfunction at  $B$ , in spite of the fact that the tangential streamlines look well-behaved in the neighborhood of the corner  $B$ .

The 2D perturbation equations for the eigenfunctions  $\theta_m(x, z)$  and  $\psi_m(x, z)$  are

$$\theta_m = -R^{-1}(\nabla^2 - k_m^2)\psi_m, \quad (39)$$

$$(\nabla^2 - k_m^2)\theta_m = \left( \frac{\partial^2}{\partial x^2} - k_m^2 \right) \psi_m. \quad (40)$$

A 2D eigenvalue problem is now formulated in the vertical  $xz$ -plane, with the following boundary conditions. The lower boundary is assumed impermeable and perfectly heat conducting

$$\psi_m = \theta_m = 0, \quad z = 0, \quad (41)$$

while the upper boundary is impermeable, with constant given heat flux

$$\psi_m = \frac{\partial \theta_m}{\partial z} = 0, \quad z = 1. \quad (42)$$

The left-hand sidewall is impermeable and thermally insulating

$$\frac{\partial \psi_m}{\partial x} = \frac{\partial \theta_m}{\partial x} = 0, \quad \text{at } x = 0, \quad (43)$$

while the right-hand sidewall is impermeable and perfectly heat conducting

$$\frac{\partial \psi_m}{\partial x} = \theta_m = 0, \quad \text{at } x = L. \quad (44)$$

This eigenvalue problem may serve as a generalization to 3D of the TNS paper [1], since  $m = 0$  should reproduce the 2D onset criterion from our previous paper.

We note that the present eigenfunction  $\Psi(x, y, z)$  for the flow is not the streamfunction of the 2D case, and it is not suited for graphical illustrations. To the following isotherm plots we will add the stagnation points where the velocity is zero. In the  $xz$ -plane these stagnation points are determined by the 2D eigenfunction by the relationships

$$\frac{\partial^2 \psi_m}{\partial x \partial z} = \left( \frac{\partial^2 \psi_m}{\partial x^2} - k_m^2 \right) \psi_m = 0. \quad (45)$$

### 3.1 On possible 2D solutions

The general 3D problem encompasses a 2D solution, which is represented by  $k = 0$  where the  $y$  dependency vanishes (infinite wavelength) and the onset mode depends only on  $x$  and  $z$ . We will now check whether this 3D problem also allows a 2D solution dependent on  $y$  and  $z$ . If so, the eigenfunctions can be written as  $\Psi = \psi_m(z) \cos(k_m y)$ ,  $\Theta = \theta_m(z) \cos(k_m y)$ . Still the sidewall boundary conditions (32)-(33) must be satisfied. From the latter condition, we find  $\Theta = 0$ , and the thermo-mechanical coupling equations implies  $\Psi = 0$ . There is no 2D solution dependent on  $y$  and  $z$  because the thermal Dirichlet condition along the right-hand sidewall forbids it. The special case  $k = 0$  of the full 3D problem gives the only 2D solution, where the flow takes place in the  $xz$ -plane.

### 3.2 Numerical solutions of the eigenvalue problem

The 3D eigenvalue problem that has been reduced to 2D by factoring out the Fourier component in the transverse  $y$  direction will now be solved numerically in the Comsol Multiphysics finite element based environment. We give the warning that there is possibly a mild singularity in the corner  $B$ . The solution will be well-behaved around the three other corners of the rectangle.

We will show plots of the lowest thermal eigenfunctions  $\Theta(x, 0, z)$  of neutral stability. The eigenfunctions with the lowest Rayleigh numbers will be displayed, for given values of the aspect ratio  $L$ . The 3D eigenfunction is given as  $\Theta(x, 0, z) = \theta_m(x, z)$ , with separate solutions for each value of the integer  $m = 0, 1, 2, \dots$ , representing the number of half wavelengths in the transverse direction once the the box width  $Y$  has been chosen. The switch between  $m = 0$  and  $m = 1$  as the preferred mode with the lowest Rayleigh number

is particularly interesting because it represents the transition from 2D to 3D marginal state of convection onset.

Each thermal eigenfunction  $\theta_m(x, z)$  gives isotherms for the perturbation temperature at the end-wall  $y = 0$ . We do not show a corresponding streamline pattern because the flow is 3D when  $m > 0$ . We will show the stagnation points where the velocity is zero. This is important for visualizing the effect of non-normal modes in the  $xz$ -plane, since the stagnation points for normal modes will always coincide with a thermal cell wall where  $\Theta = 0$ . It will be interesting to depict the stagnation points for each thermo-mechanical eigenfunction, to observe how far it is displaced away from a border isotherm  $\Theta = 0$  between a cold downwelling domain and a warm upwelling domain.

### 3.2.1 A square cross-section $L = 1$

We will study the case  $L = 1$ , choosing  $Y = 1$  which gives the geometry of a cube, where  $k_m = m\pi$  ( $m = 0, 1, 2, \dots$ ). We will benchmark the present solution with respect to the case  $m = 0$  which represents 2D flow, already solved in the TNS paper [1] with a somewhat different approach since the 2D streamfunction does not exist in the present general 3D problem. In *Figure 3* we show this 2D case, to be compared with the Rayleigh numbers found for the lowest eigenfunctions shown in *Figure 2* of the TNS paper [1];  $R = 36.719$ ,  $R = 65.142$ ,  $R = 114.18$ ,  $R = 142.2$ , respectively. Our calculated values are  $R = 36.72$ ,  $R = 65.16$ ,  $R = 114.23$ ,  $R = 142.25$ , giving acceptable agreement with the previous TNS computations [1]. We introduce green circles to mark the stagnation points for the flow of each marginal eigenfunction. The stagnation points of the TNS paper [1] can be identified as centers of recirculating flow domains, giving good agreement with our *Figure 3*.

It is desirable to get a visual impression of non-normal modes for comparison with normal modes. For this purpose, we consider the displacements between the green circles (stagnation points) and their neighboring dividing isotherms (yellow) defined by  $\theta = 0$ . These displacements are significant since a normal-mode solution will have its stagnation points in a vertical plane coinciding with the dividing isotherms (where  $\theta = 0$ ). These dividing isotherms will be horizontal and/or vertical if the eigenfunction is of the normal-mode type in all spatial directions, eventually apart from one. One single spatial direction with non-normal mode dependency remains consistent with the separation of variables. Two or three directions of non-normal mode dependency will violate the separation of variables, which is required for obtaining dividing isotherms parallel to the coordinate axes.

In *Figure 4* we keep the value  $L = 1$ , showing our first genuinely 3D onset mode  $m = 1$  where  $k_1 = \pi$ . This mode is preferred at the expense of the 2D mode of *Figure 5* because its Rayleigh number  $R = 32.26$  is smaller than the value  $R = 36.72$  of the preferred 2D mode shown in *Figure 3*. A remarkable feature of the lowest mode of *Figure 4* is that the whole thermal eigenfunction at  $y = 0$  is positive, with no cold domain at all. This is a plausible behavior because of the half-wavelength dependency inside the box along the

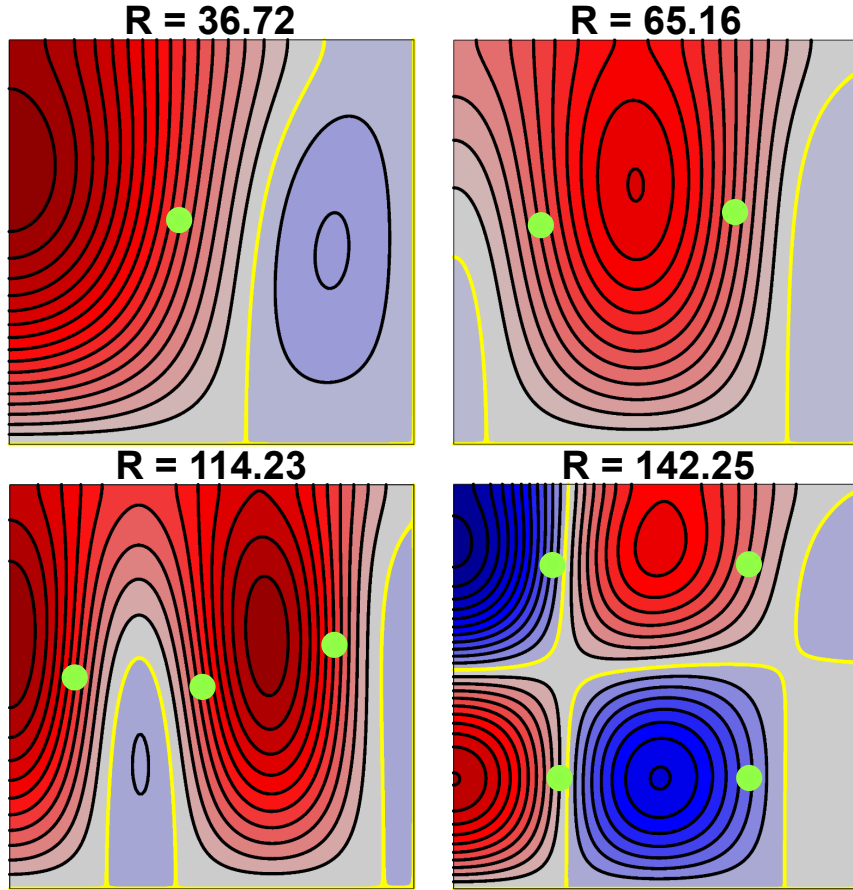


**Fig. 3** Isotherms for the four first thermal eigenfunctions for  $L = 1$  with  $m = 0$ . Black lines represent isotherms. Dividing isotherms  $\theta_0(x, z) = 0$  marked with yellow represent the borders between warm and cold domains. Stagnation points for the flow are marked by green circles.

$y$  direction. Thus the thermal eigenfunction at  $y = Y$  is negative. The regular local balance between a hot upwelling domain and a cold downwelling domain within a vertical cross-section of a convection cell is here replaced with an anti-symmetric thermal balance between the end-walls of the box.

In *Figure 5* we show the isotherms for the four lowest eigenfunctions with  $L = 1$ , considering the second lateral mode  $m = 2$ , where there is a full wavelength dependency in the lateral  $y$  direction. The lowest Rayleigh number is here much higher than the previous cases  $m = 0$  and  $m = 1$ . *Figure 5* show stagnation points that are closer to the dividing isotherms than in the previous figures. Any stagnation point with a central position in the rectangle will be very close to a dividing isotherm.

We note that the value  $Y = 1$  (with  $m = 2$ ) chosen in *Figure 5* is equivalent to the parameter combination  $Y = 0.5$ ,  $m = 1$ . When we compare the *Figures*

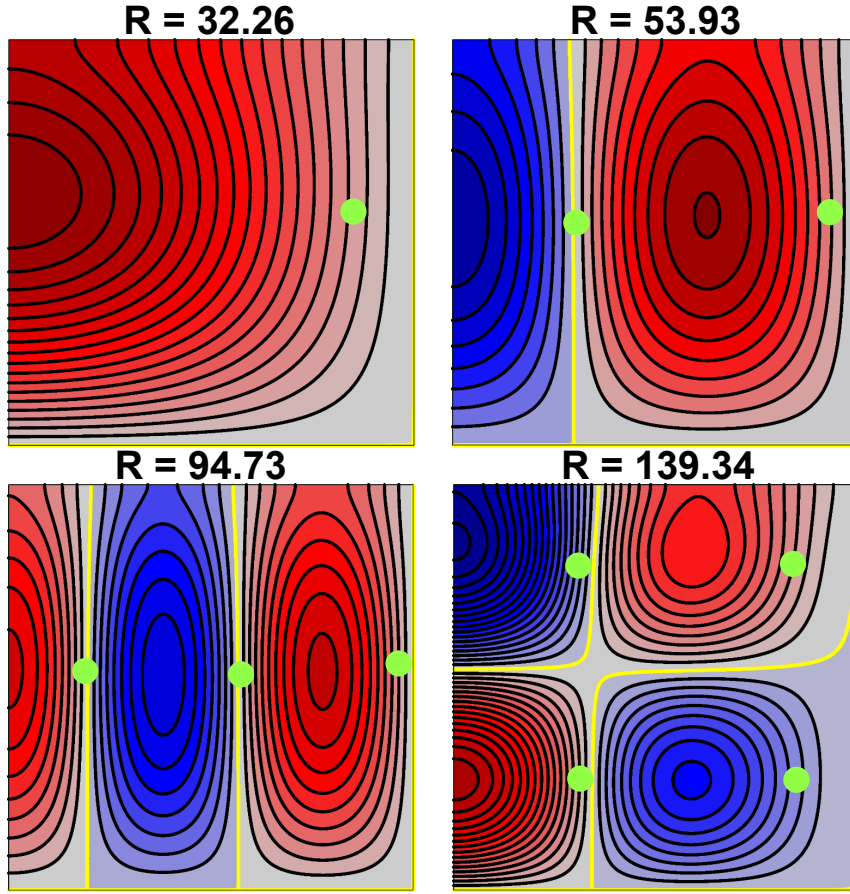


**Fig. 4** Isotherms for the four first thermal eigenfunctions for  $L = 1$  with  $m = 1$  ( $Y = 1$ ). Black lines represent isotherms. Dividing isotherms  $\theta_1(x, z) = 0$  marked with yellow represent the borders between warm and cold domains. Stagnation points for the flow are marked by green circles.

3-5, we observe that the isotherm patterns tend to be more regular for 3D flow ( $m > 0$ ) than for 2D flow ( $m = 0$ ). The 3D eigenfunctions seem to be smoothed due to their normal-mode dependency in the lateral  $y$  direction.

### 3.2.2 A tall cross-section $L = 0.5$

Figure 6 shows the 3D thermal eigenfunctions for  $m = 1$  and  $m = 2$ , represented at the end-wall  $y = 0$ . We omit the 2D case  $m = 0$ , where the onset of convection takes place at  $R = 65.216$  (calculated in the TNS paper [1]). 3D convection is preferred, since the first lateral mode  $m = 1$  gives the critical Rayleigh number  $R = 44.38$ . The clearest non-normal mode behavior occurs for  $m = 1$ , with strongly curved dividing isotherms (yellow) for the third and fourth eigenfunction. Significant displacements are observed between stagna-

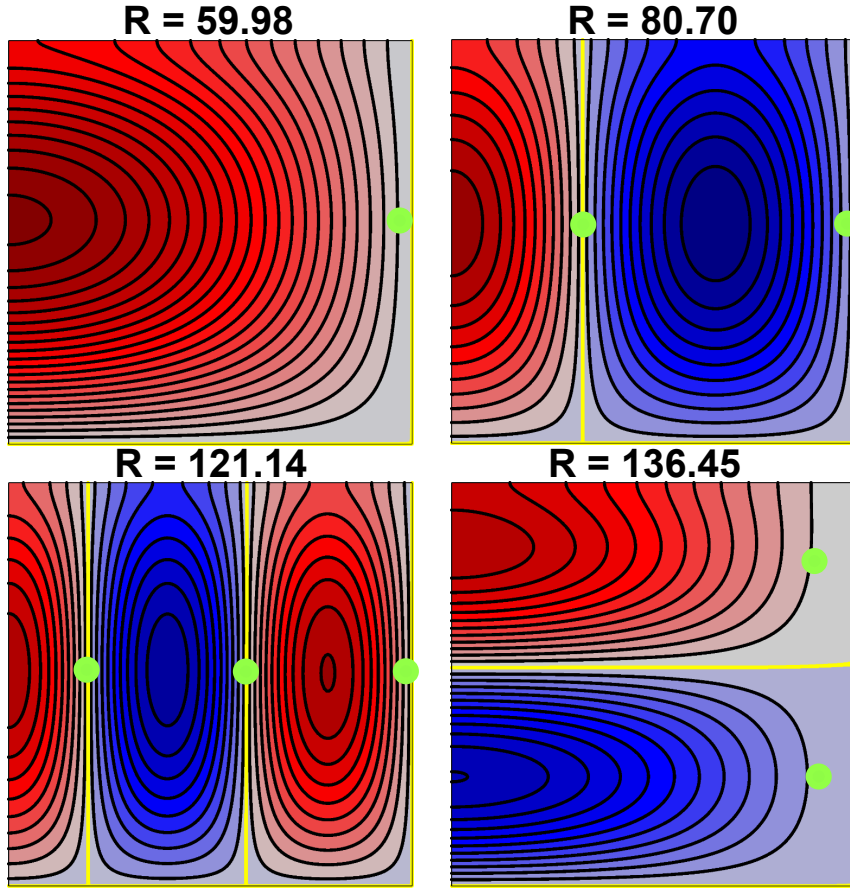


**Fig. 5** Isotherms for the four first thermal eigenfunctions for  $L = 1$  with  $m = 2$  ( $Y = 1$ ). Black lines represent isotherms. Dividing isotherms  $\theta_2(x, z) = 0$  marked with yellow represent the borders between warm and cold domains. Stagnation points for the flow are marked by green circles.

tion points and curved dividing isotherms. The second lateral mode  $m = 2$  for the eigenfunction behaves more regularly.

### 3.2.3 A moderately long cross-section $L = 2$

The case  $L = 2$  is represented in *Figure 7*, where the lowest Rayleigh number of 2D convection is  $R = 29.676$ , found in the TNS paper [1]. The first lateral mode  $m = 1$  for  $Y = 1$  gives a higher value  $R = 29.81$ , which means that 2D convection is preferred, different from the above cases  $L = 1$  and  $L = 0.5$ . The isotherms are quite regular for this case, not differing much from normal modes. This is also confirmed by the fact that most of the stagnation points are located near the respective dividing isotherms (where  $\theta = 0$ ).

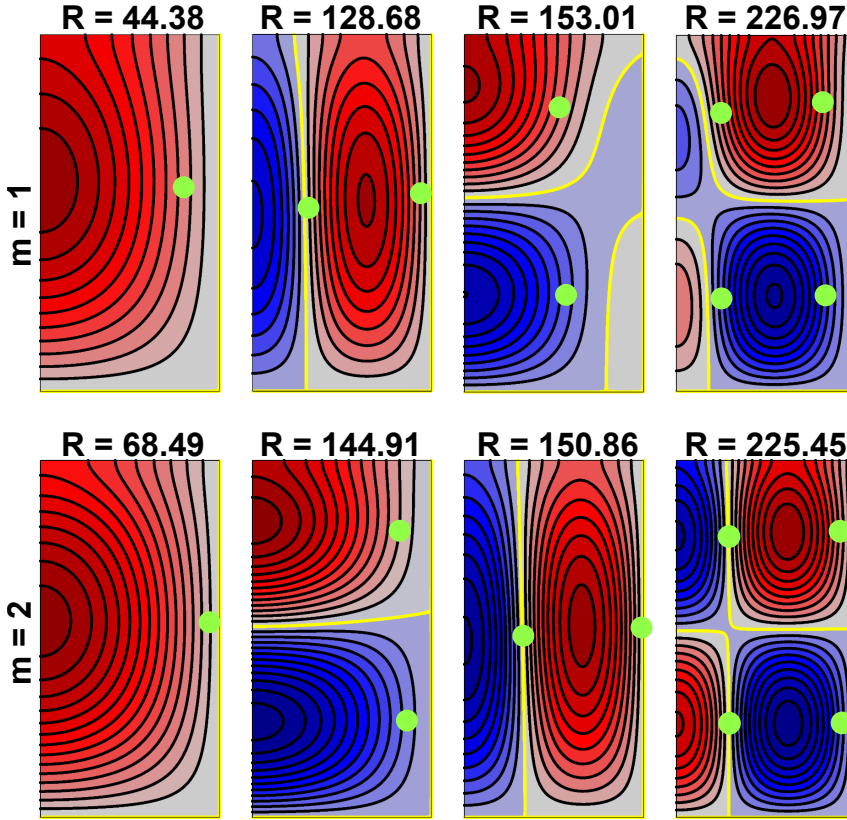


**Fig. 6** Isotherms for the four first thermal eigenfunctions for  $L = 0.5$  and  $Y = 1$  with  $m = 1$  (top) and  $m = 2$  (bottom), respectively. Black lines represent isotherms. Dividing isotherms  $\theta_2(x, z) = 0$  marked with yellow represent the borders between warm and cold domains. Stagnation points for the flow are marked by green circles.

### 3.3 A continuous spectrum for the lateral mode

So far, we have considered a given dimensionless width  $Y$  of the porous box in the  $y$  direction, with the discrete spectrum of legal wavenumbers  $k_m$  for the lateral wavenumber. We will now discuss the dispersion relation, which shows how the eigenvalue  $R$  depends on a continuous spectrum of lateral wavenumbers  $k$ , which are allowed in the limit of a semi-infinite box width  $L$ . We will search for the global minimum of the Rayleigh number. We will also determine precisely the switch between 2D and 3D preferred mode of convection onset, at the wavenumber  $k^*$ . For these purposes, we need to consider a continuous spectrum for  $k$ .

Figure 8 shows the Rayleigh number for the lowest mode of convection, giving its variation with respect to the continuously varying lateral wavenumber  $k$ . The global minimum  $R = R_c$  with its associated wavenumber  $k_c$  are shown in Figure 8, and also the parameter combination  $(R^*, k^*)$  where the

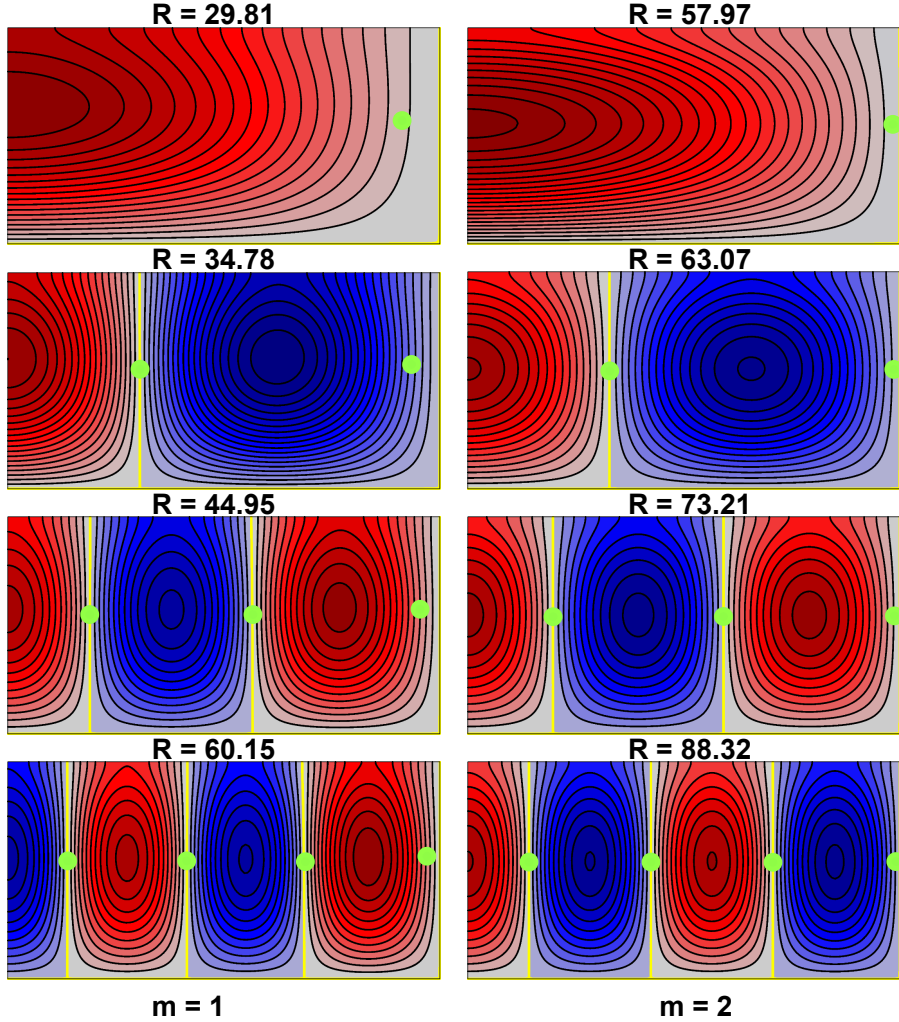


**Fig. 7** Isotherms for the four first thermal eigenfunctions for  $L = 2$  and  $Y = 1$  with  $m = 1$  (left) and  $m = 2$  (right), respectively. Black lines represent isotherms. Dividing isotherms  $\theta_2(x, z) = 0$  marked with yellow represent the borders between warm and cold domains. Stagnation points for the flow are marked by green circles.

onset mode switches between 2D and 3D. The existence of the global minimum implies that there is a finite wavenumber above which the solution is 3D.

Similar transitions from 2D to 3D onset modes in a porous box have been studied by Barletta and Storesletten [10]. Their calculated transition values  $k^*(L)$  comparable with our *Figure 8* are  $k^*(0.5) = 6.823$ ,  $k^*(1) = 4.783$ ,  $k^*(2) = 3.928$ . Physically, the model by Barletta and Storesletten [10] differs from the present model with respect to only one boundary condition, which is the thermal condition at the upper boundary, where we let a Neumann

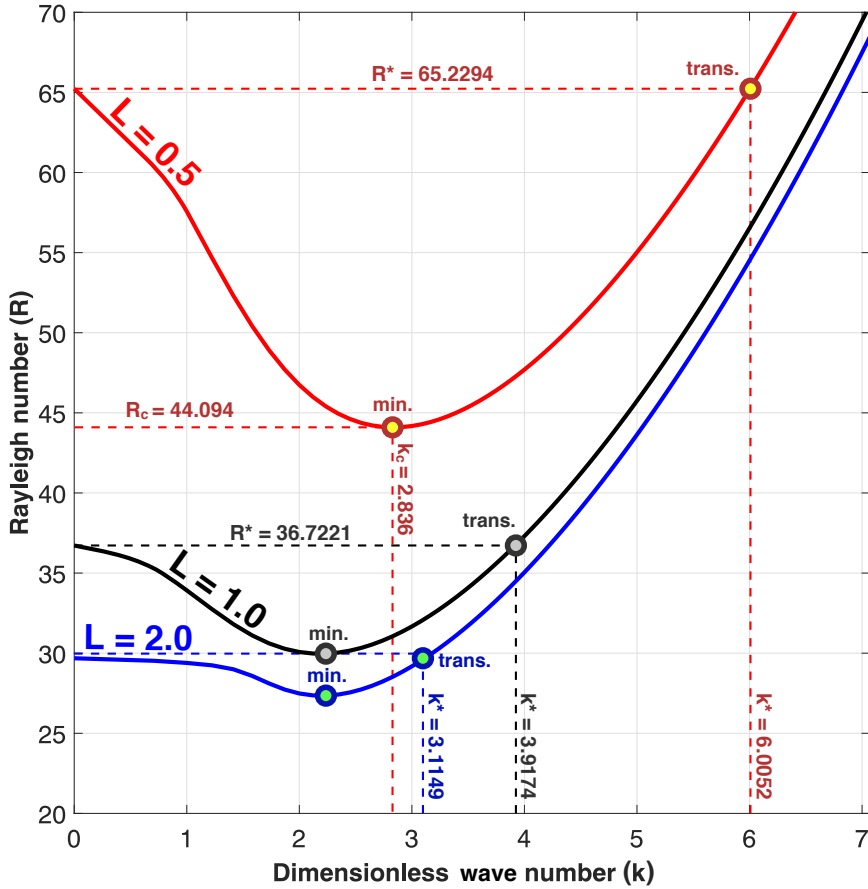


**Fig. 8** Lowest Rayleigh number ( $R$ ) as continuous function of the lateral dimensionless wavenumber  $k$ , with  $L = 0.5$ ,  $L = 1$  and  $L = 2$ , respectively. The global minimum Rayleigh numbers  $R_c$  are marked with circles, and also the transition points  $(k^*, R^*)$  where the onset mode switches from 2D to 3D. In the text these points are compared with related computations by Barletta and Storesletten [10].

condition replace their Dirichlet condition. All other thermal and mechanical boundary conditions may be considered as identical, with one crucial reservation: Their vertical  $yz$ -plane must then obey a symmetry condition, which may or may not be the case, since  $x = 0$  in their model is a mid-plane between the two sidewalls and not an external boundary. The preferred mode of convection must then be symmetric around the  $x$  axis in the model of Barletta and Storesletten [10], which it is for their displayed eigenfunctions. Their notation  $s$  for the aspect ratio will then correspond to  $L$  in our present model. Barletta and Storesletten [10] gave no proof that their preferred 3D eigenfunctions are always symmetric. In this context, it is interesting to note that the 2D case (Nilsen and Storesletten [9]) has a degeneracy where the symmetric

and antisymmetric eigenfunctions have coinciding Rayleigh numbers. Rees and Lage [11] confirmed these results. This degeneracy was explained by Rees and Tyvand [12] by separating out a horizontal Fourier component with arbitrary phase, reducing the fourth-order eigenvalue problem to a second-order problem governed by a Helmholtz equation. The separation of the Fourier components responsible for the degeneracy implies that symmetry or anti-symmetry of the eigenfunctions around the mid-plane are two equivalent special cases.

*Figure 8* offers a comparison with the results from Barletta and Storesletten [10] concerning the transition from 2D to 3D onset mode of convection. It shows that our results for  $k^*$  are systematically more than 10 % below those of Barletta and Storesletten [10]. This is reasonable because our thermal Neumann condition at the upper boundary is known to reduce the preferred wavenumber of the classical HRL problem significantly, from  $\pi$  to 2.33 (Nield [8]).

*Figure 8* gives the continuous dispersion relation  $(k, R)$  for the non-normal mode with the lowest Rayleigh number. The three values  $L = 0.5$ ,  $L = 1$  and  $L = 2$  for the aspect ratio were chosen because these values have been picked for the isotherm plots above. We will now take a step further in investigating how the important wavenumbers  $k_c$  and  $k^*$  vary with the aspect ratio  $L$ . This is done in *Figure 9* and *Figure 10*. These figures represent two important combinations of onset Rayleigh number and the associated wavenumber: First the onset value of  $R$  with the smallest wavenumber  $k^*$  in the  $y$  direction that gives a 3D onset mode to be preferred at the expense of the 2D solution of the TNS paper [1]. However, when  $k$  is increased further beyond  $k^*$ , there is another value  $k_c$  that will give the global minimum  $R_c$  for the Rayleigh number of 3D convection. These two sets of Rayleigh numbers are put together in *Figure 9* as functions of  $L$ , and their respective wavenumber of onset are given as functions of  $L$  in *Figure 10*. The graphs for  $R_c(L)$  and  $k_c(L)$  in *Figures 9–10* approach the asymptotic limit values  $(R, k) \rightarrow (27.10, 2.33)$  as  $L \rightarrow \infty$ . These results are known from Nield [8].

*Table 1* gives selected numerical evaluations corresponding to *Figures 9–10*. We repeat our chosen values for the eigenfunction plots above, and add very small and very large values of  $L$ . The only asymptotic result available for benchmarking are those from Nield [8], fitting well with our computed values for  $L = 100$  and  $L = 1000$ . An intriguing coincidence in *Table 1* is that  $Y^*$  seems to approach  $L$  when  $L \ll 1$ , but we have not been able to argue analytically for this apparently simple relationship.

In *Figure 11* we return to consider a finite box width  $Y$ . We display the transitional box width  $Y^* = \pi/k^*$  and the critical box width  $Y_c = \pi/k_c$  (implied by *Figure 10*) as functions of  $L$ . A physical interpretation of *Figure 11* goes as follows. For each given value of  $L$ , we start with zero width  $Y$  and increase it until a value  $Y^*$  is reached, above which the onset mode is 3D. For all  $Y < Y^*$  the onset mode is 2D as in the TNS paper [1]. If we increased  $Y > Y^*$  further, we would arrive at a value  $Y_c$  where the global minimum for  $R$  is first reached, but this minimum value will repeat itself for all values  $Y = nY_c$ , where  $n$  is an integer greater than one.

**Table 1** Evaluations of the wavenumbers  $k = k_c$  and  $kl = k^*$  for selected values of  $L$ , with the associated Rayleigh numbers  $R$  of convection onset and the shortest associated box widths  $Y = \pi/k$ .

	$L = 0.001$	$L = 0.01$	$L = 0.5$	$L = 1$	$L = 2$	$L = 10$	$L = 100$	$L = 1000$
$R_c$	2.6787E6	2.5671E4	44.094	29.966	27.346	27.109	27.126	27.091
$k_c$	68.6273	21.0554	2.8364	2.1886	2.1981	2.3195	2.3070	2.3159
$Y_c$	0.0458	0.1492	1.1076	1.4355	1.4292	1.3544	1.3617	1.3566
$R^*$	1.0174E7	1.0138E5	65.229	36.722	29.685	27.325	27.944	28.111
$k^*$	2.745E3	276.6080	6.0052	3.9174	3.1149	2.5592	2.8060	2.8680
$Y^*$	0.0011	0.0114	0.5232	0.8020	1.0086	1.2275	1.1196	1.0954

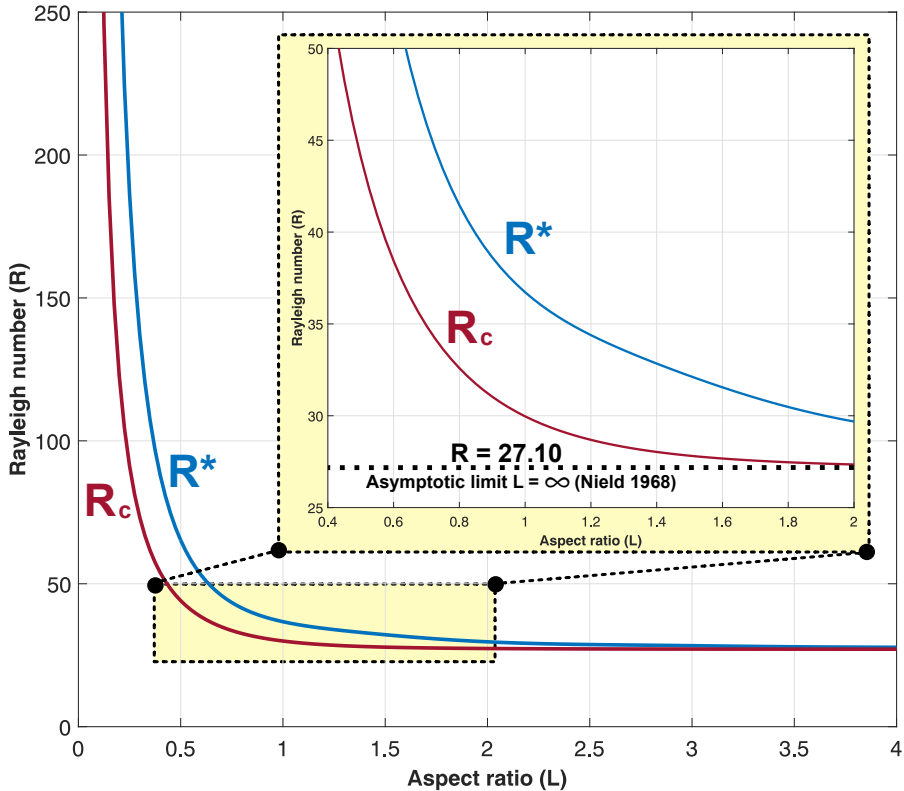


**Fig. 9** Rayleigh number ( $R$ ) as a function of the aspect ratio ( $L$ ) for both the global minimum  $R_c$  and the transition value  $R^*$ .

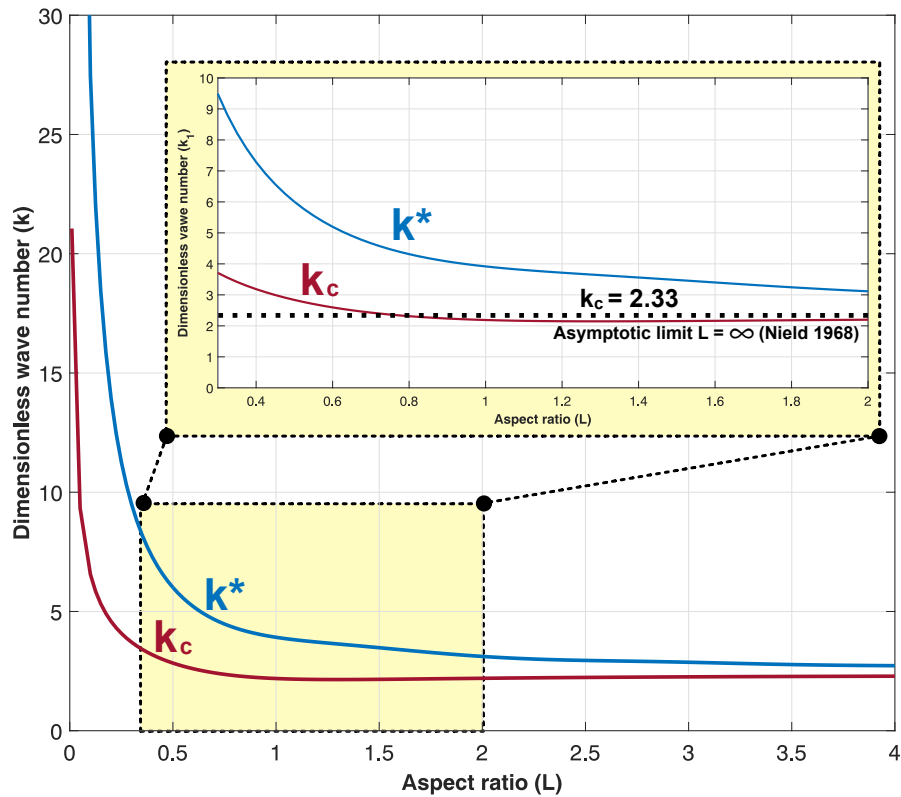


**Fig. 10** Dimensionless wavenumber ( $k = k_1$ ) as a function of the aspect ratio ( $L$ ) for both the global minimum ( $R_c, k_c$ ) and the transition value ( $R^*, k^*$ ).

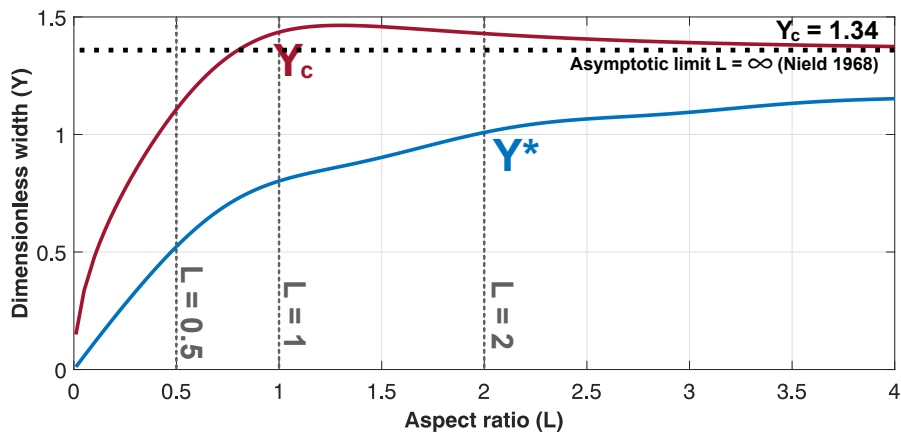


**Fig. 11** Dimensionless width  $Y$  as a function of the aspect ratio  $L$  for both the global minimum ( $R_c, k_c$ ) (where  $Y_c = \pi/k_c$ ) and the transition value ( $R^*, k^*$ ) (where  $Y^* = \pi/k^*$ ).

#### 4 Summarizing discussion

The focus of the present work is the threshold of transition between 2D and 3D eigenfunctions for a rectangular box of porous medium heated uniformly from below. No such analysis has been reported with 2D non-normal modes over a rectangular cross-section area. In fact, the first work on a similar transition between 2D and 3D eigenfunctions was published by Storesletten and Tveitereid [3]. They investigated a wrapped horizontal cylinder with conducting cylinder walls and adiabatic end-walls. When  $L < 0.86$  the preferred eigenfunction is 2D, and when  $L > 0.86$  the preferred eigenfunction is 3D.

Nilsen and Storesletten [9] provided the first solution of a 2D Horton-Rogers-Lapwood (HRL) problem with non-normal mode dependency in the horizontal direction. Moreover, Barletta and Storesletten [10] generalized this model to 3D, by including a cross-wise Fourier mode satisfying conditions of adiabatic and impermeable end-walls. The present problem is similar to the 3D box problem considered by Barletta and Storesletten [10], as 11 out of 12 thermo-mechanical boundary conditions along the six boundary planes are in common, assuming that the preferred onset mode of Barletta and Storesletten [10] is symmetric around their mid-plane  $x = 0$ . Their 3D onset wavenumber in the  $y$  direction is roughly ten percent above the values found in the present work, which is reasonable since only one out of 12 boundary conditions differs in these two models.

The single thermal condition of given heat flux at the upper boundary makes our model distinguishable from the previous work on 3D convection onset in porous boxes. In addition, this thermal Neumann condition has mathematical implications, since it forbids analytical solutions of the eigenvalue problem. One immediate complication of the present model is that the dividing isotherms between bordering thermal cells will neither be exactly horizontal nor vertical. This is because a non-normal mode eigenfunction in 2D or 3D is non-separable in space, and in fact, no formulation of a 1D eigenvalue problem is possible.

A few papers are devoted to the transition from 2D to 3D onset modes of convection. Barletta *et al.* [13] made a similar analysis to the present one for a 3D porous box problem where the side boundaries are permeable and conducting, but these boundary conditions differ too much from ours for the sake of detailed comparisons.

Our results indicate that the inclusion of a transverse Fourier mode produces 3D eigenfunctions of more regular shapes than the strictly 2D non-normal modes. This is reasonable because the additional lateral Fourier component is itself a normal mode component. We have identified some cases where the 2D non-normal mode in a cross-sectional plane of a 3D eigenfunction has only positive perturbation temperatures, which is a behavior that would not occur for strictly 2D instability. The warm fluid at one end-wall achieves balance with the cold fluid at the other end-wall for the lowest transverse mode that covers half a wavelength within the porous box.

In this paper, we have studied the effect of increasing the width of  $Y$  between the adiabatic end-walls of the porous box. The thermo-mechanical eigenfunction is 2D when  $Y$  is small. When  $Y$  exceeds a threshold value of  $Y^*(L)$ , the preferred eigenfunction is 3D. The critical Rayleigh number for the 3D perturbations continues to decrease when  $Y$  is increased beyond  $Y^*$ . At a value  $Y_c(L)$  above  $Y^*$  the lowest (global) Rayleigh number  $R_c$  is achieved. In fact, this value of  $R$  is identical to the onset criterion for an infinitely wide porous box, where the preferred wavelength of transverse disturbance is  $2Y_c$ .

Non-normal modes is not an established concept in the theory of Rayleigh-Bénard convection, albeit arising naturally for boundary conditions physically rich enough to defy separation of variables in space. The literature on the Rayleigh-Bénard onset problem has normal modes as its analytical basis, implicitly reducing the effective spatial order of the eigenvalue problem from four to two. The full fourth-order problem has non-normal modes in 2D once two boundary conditions meeting at corners are in mutual conflict there. This should be considered as a standard situation from a physical point of view, even though it has not yet been addressed properly mathematically. Weak singularities can be expected at corners where meeting boundary conditions do not match, and our numerical solution is at best a good approximation for the outer solution in the context of matched asymptotic expansions. However, integrated quantities like the onset Rayleigh number are likely to be unaffected by such weak singularities, as they show good convergence according to our present calculations.

## References

1. Tyvand, P.A., Nøland, J.K. and Storesletten, L. (2019) A non-normal-mode marginal state of convection in a porous rectangle. *Transp. Porous Med.* **128**, 633-651. Referred to in the text as the TNS paper.
2. Moffatt, H.K. (1964) Viscous and resistive eddies near a sharp corner. *J. Fluid Mech.* **18**, 1-18.
3. Storesletten, L. and Tveitereid, M. (1991) Natural convection in a horizontal porous cylinder. *Int. J. Heat Mass Transf.* **34**, 1959-1968.
4. Horton, C.W. and Rogers, F.T. (1945) Convection currents in a porous medium. *J. Appl. Phys.* **16**, 367-370.
5. Lapwood, E.R. (1948) Convection of a fluid in a porous medium. *Proc. Camb. Phil. Soc.* **44**, 508-521.
6. Wooding, R.A. (1959) The stability of a viscous liquid in a vertical tube containing porous material. *Proc. R. Soc. Lond.* **A252**, 120-134.
7. Beck, J.L. (1972) Convection in a box of porous material saturated with fluid. *Phys. Fluids* **15**, 1377-1383.
8. Nield, D.A. (1968) Onset of thermohaline convection in a porous medium (Appendix). *Water Resources Res.* **11**, 553-560.
9. Nilsen, T. and Storesletten, L. (1990) An analytical study on natural convection in isotropic and anisotropic porous channels. *ASME J. Heat Transf.* **112**, 396-401.
10. Barletta, A. and Storesletten, L. (2012) A three-dimensional study of the onset of convection in a horizontal, rectangular porous channel heated from below. *Int. J. Therm. Sci.* **55**, 1-15.
11. Rees, D.A.S. and Tyvand, P.A. (2004) The Helmholtz equation for convection in two-dimensional porous cavities with conducting boundaries. *J. Eng. Math.* **490**, 181-193.

12. Rees, D.A.S. and Lage, J.L. (1996) The effect of thermal stratification on natural convection in a vertical porous insulation layer. *Int. J. Heat Mass Transf.* **40**, 111-121.
13. Barletta, A., Rossi di Schio, E. and Storesletten, L. (2013) Convective instability in a horizontal porous channel with permeable and conducting side boundaries. *Transp. Porous Med.* **99**, 515-533.